

Theoretical Elucidation of Kinetic and Thermodynamic Control of Radical Addition Regioselectivity

Andrew G. Leach, Renxiao Wang, G. Erich Wohlhieter, Saeed I. Khan,
Michael E. Jung,* and K. N. Houk*

Contribution from the Department of Chemistry and Biochemistry, University of California,
Los Angeles, California 90095-1569

Received November 14, 2002; E-mail: houk@chem.ucla.edu

Abstract: The cyclizations of two structurally similar 2-oxo-5-hexenyl-type radicals have been investigated by ab initio and density functional (UB3LYP/6-31+G**//UHF/6-31G* and UB3LYP/6-31G*/UB3LYP/6-31G*) calculations. The origin of apparently contradictory reports of 6-endo and 5-exo cyclizations is determined. Kinetic control favors 6-endo cyclization, while thermodynamic control gives 5-exo cyclization, and the observation of different products from different research groups arises from the difference in experimental conditions used by the two groups. The outcome of a new cyclization reaction was predicted by using these theoretical techniques. Kinetic control is predicted to yield exclusively the products of 6-endo cyclization, while thermodynamic control would lead to an approximately equal mixture of one 6-endo and one 5-exo cyclized product. Experimental studies revealed that the reaction yields only the products of 6-endo cyclization through kinetic control.

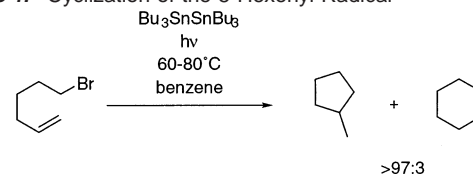
Introduction

The intramolecular additions of radicals to carbon–carbon double bonds to form five- or six-membered rings are of continuing interest in synthetic organic chemistry.^{1,2} Generally, 5-hexenyl radicals cyclize with high regioselectivity to give five- rather than six-membered rings (Scheme 1).³

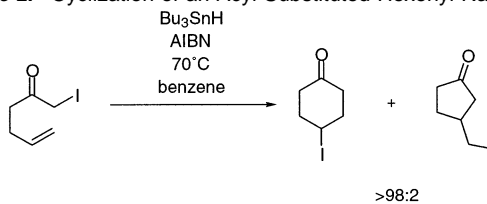
This is a mainstay of Baldwin's rules, which note that 5-exo cyclization should be preferred over 6-endo for attack on a trigonal center.⁴ Two force field models have been developed which enable quantitative predictions of these regioselectivities to be made.⁵ In contrast to Baldwin's rules, the intramolecular cyclizations of radicals adjacent to endo carbonyls ("acyl-substituted radicals") have been found to yield 6-endo products (Scheme 2).⁶ Several factors (both electronic and steric) contribute to this preference,⁷ and a force field model has been developed which accounts for these in a quantitative fashion.⁸

Recently, Jung and Rayle⁹ and Haney and Curran² reported experimental intramolecular radical additions that revealed puzzling differences in this type of regioselectivity. Although the reactants employed are quite similar (Schemes 3 and 4),

Scheme 1. Cyclization of the 5-Hexenyl Radical³



Scheme 2. Cyclization of an Acyl-Substituted Hexenyl Radical⁷

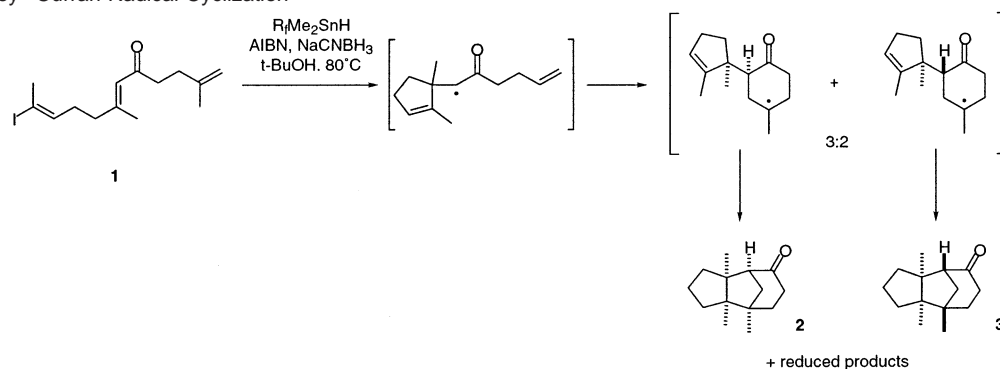
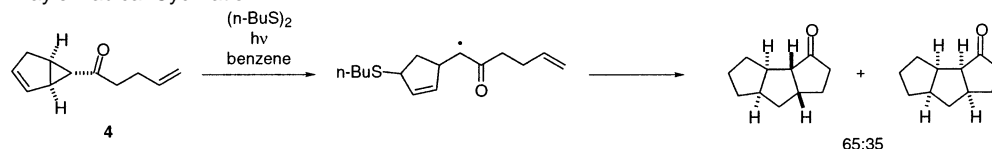


strikingly different product mixtures were obtained. Haney and Curran's experiments, in which the reaction is initiated by the combination of tin hydride with vinyl iodide **1**, yield the 6-endo derived products **2** and **3** in line with expectation for this type of radical.

However, Jung and Rayle's intramolecular radical additions, initiated by thiyl radical addition to vinyl cyclopropane **4**, gave a preponderance of the 5-endo pathway instead (Scheme 4). Curran and Haney suggested that the radical cyclizations might be reversible under these conditions and that the product could be the result of thermodynamic control.²

To determine energetics and the nature of the transition states, products, and intermediates for these processes, quantum mechanical calculations have been employed. Such calculations have been found to be a useful tool for understanding the selectivity of radical reactions,^{10,11} and we have employed them

- (1) (a) Bennasar, M.-L.; Juan, C.; Bosch, J. *Chem. Commun.* **2000**, 2459–2460. (b) Ellis, D. A.; Hart, D. J.; Zhao, L. *Tetrahedron Lett.* **2000**, 41, 9357–9360. (c) Snider, B. B.; Buckman, B. O. *J. Org. Chem.* **1992**, 57, 4883–4888.
- (2) Haney, B. P.; Curran, D. P. *J. Org. Chem.* **2000**, 65, 2007–2013.
- (3) Walling, C.; Cioffari, A. *J. Am. Chem. Soc.* **1972**, 94, 6059–6064.
- (4) Baldwin, J. E. *J. Chem. Soc., Chem. Commun.* **1976**, 734–746.
- (5) (a) Beckwith, A. L. J.; Schiesser, C. H. *Tetrahedron Lett.* **1985**, 26, 373–376. (b) Beckwith, A. L. J.; Schiesser, C. H. *Tetrahedron* **1985**, 41, 3925–3941. (c) Spellmeyer, D. C.; Houk, K. N. *J. Org. Chem.* **1987**, 52, 959–974.
- (6) Clive, D. L. J.; Cheshire, D. R. *J. Chem. Soc., Chem. Commun.* **1987**, 1520–1523.
- (7) Curran, D. P.; Chang, C.-T. *J. Org. Chem.* **1989**, 54, 3140–3157.
- (8) Broeker, J. L.; Houk, K. N. *J. Org. Chem.* **1991**, 56, 3651–3655.
- (9) Jung, M. E.; Rayle, H. L. *J. Org. Chem.* **1997**, 62, 4601–4609.

Scheme 3. Haney–Curran Radical Cyclization²**Scheme 4.** Jung–Rayle Radical Cyclization⁹

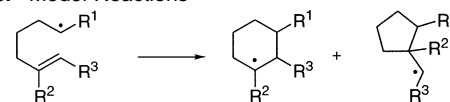
to explain these dichotomous experimental results and to predict the outcome of a similar reaction.

Computational Methodology

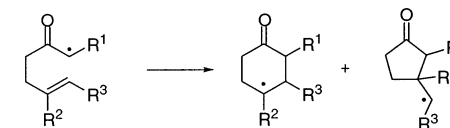
Two levels of theory have been employed. Using Hartree–Fock geometries but evaluating energies with a method which accounts for correlation has previously been shown to be effective for radical reactions.^{5c,11} Thus, the UB3LYP/6-31+G**//UHF/6-31G* method was used throughout. To assess this methodology, the same species were optimized with UB3LYP/6-31G* in some cases, and the corresponding UB3LYP/6-31G* energies were compared to those obtained with the computationally less demanding method already described.¹² All calculations were performed using the Gaussian98 program,¹³ and all stationary points were analyzed through computation of their vibrational frequencies. Reported energies include a thermal correction to 298 K based on the UHF (UB3LYP//UHF method) or UB3LYP (UB3LYP//UB3LYP method) frequencies.

Results

(1) Model Reaction Study of Intramolecular Additions of Alkyl and Acyl-Substituted Radicals. Initially, the cyclizations of four model reactants, **5**, **6**, **7**, and **8**, were studied. These reactions were chosen to investigate the regioselectivity for the cyclization of alkyl radicals and the effect of introducing alkyl substituents at C1, C5, and C6. Similarly, **9**, **10**, **11**, and **12**, were used to study the intramolecular additions of radicals α to carbonyls (Scheme 5).

Scheme 5. Model Reactions

- 5**; R¹=H, R²=H, R³=H
6; R¹=Me, R²=H, R³=H
7; R¹=H, R²=Me, R³=H
8; R¹=H, R²=H, R³=Me



- 9**; R¹=H, R²=H, R³=H
10; R¹=Me, R²=H, R³=H
11; R¹=H, R²=Me, R³=H
12; R¹=H, R²=H, R³=Me

Table 1. UB3LYP/6-31+G(d,p)//UHF/6-31G(d) Energetics of Intramolecular Additions of Alkyl-Substituted Radicals to Alkenes^a

reactant	6-endo pathway		5-exo pathway		endo/exo (expt)	endo/exo (calcd)
	chair TS	boat TS	chair TS	boat TS		
5	9.1	11.6	6.4	8.1	2:98 ¹⁴ , <1:>99 ³	1:99
6	9.6	12.2	7.0	8.7	1:99 ¹⁴	1:99
7	8.4	10.7	9.1	10.3	60:40 ^{14,15}	75:25
8	9.8	12.5	6.5	8.1	<1:>99 ¹⁶	<1:>99

^a Energies are in kcal/mol. The reactant in the all-anti conformation is taken as reference.

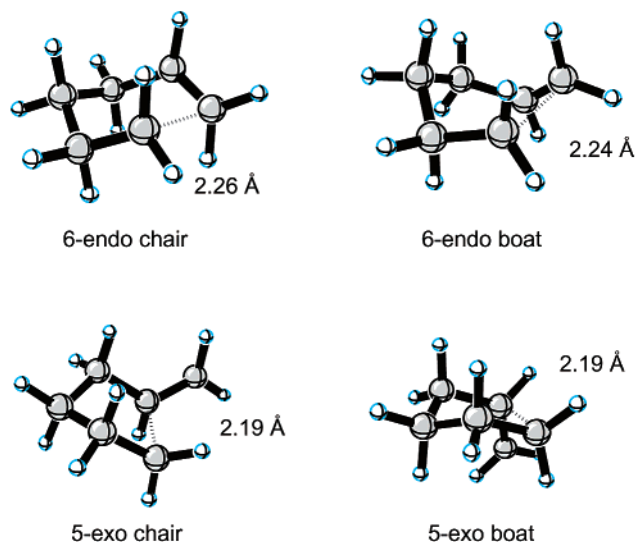
Transition states in different conformations were identified for each reaction. In the following sections, these transition states will be named chair, boat, or twist-boat, after the arrangement of C1–C2–C3–C4–C5–C6 even for species leading to five-membered ring products.^{5c} The results for the alkyl radical addition reactions of **5** to **8** are summarized in Table 1, and the results for **9** to **12** are summarized in Table 2. The kinetic 6-endo/5-exo regioselectivity in each model reaction was assumed to depend on the relative activation energies of cyclization in the two series and was calculated from a Boltzmann distribution over all relevant transition states obtained from these calculations.

- (10) (a) Houk, K. N.; Paddon-Row, M. N.; Spellmeyer, D. C.; Rondan, N. G.; Nagase, S. *J. Org. Chem.* **1986**, *51*, 2874–2879. (b) Olivella, S.; Solé, A. *J. Am. Chem. Soc.* **2000**, *122*, 11416–11422.
 (11) Wong, M. W.; Radom, L. *J. Phys. Chem.* **1995**, *99*, 8582–8588.
 (12) B3LYP utilizes Becke's three-parameter exchange functional and the Lee–Yang–Parr correlation functional. Becke, A. D. *J. Chem. Phys.* **1993**, *98*, 5648 and Lee, C.; Yang, W.; Parr, R. G. *Phys. Rev. B* **1988**, *37*, 785.
 (13) Frisch, M. J.; Trucks, G. W.; Schlegel, H. B.; Scuseria, G. E.; Robb, M. A.; Cheeseman, J. R.; Zakrzewski, V. G.; Montgomery, J. A., Jr.; Stratmann, R. E.; Burant, J. C.; Dapprich, S.; Millam, J. M.; Daniels, A. D.; Kudin, K. N.; Strain, M. C.; Farkas, O.; Tomasi, J.; Barone, V.; Cossi, M.; Cammi, R.; Mennucci, B.; Pomelli, C.; Adamo, C.; Clifford, S.; Ochterski, J.; Petersson, G. A.; Ayala, P. Y.; Cui, Q.; Morokuma, K.; Malick, D. K.; Rabuck, A. D.; Raghavachari, K.; Foresman, J. B.; Cioslowski, J.; Ortiz, J. V.; Stefanov, B. B.; Liu, G.; Liashenko, A.; Piskorz, P.; Komaromi, I.; Gomperts, R.; Martin, R. L.; Fox, D. J.; Keith, T.; Al-Laham, M. A.; Peng, C. Y.; Nanayakkara, A.; Gonzalez, C.; Challacombe, M.; Gill, P. M. W.; Johnson, B. G.; Chen, W.; Wong, M. W.; Andres, J. L.; Head-Gordon, M.; Replogle, E. S.; Pople, J. A. *Gaussian 98*, revision A.7; Gaussian, Inc.: Pittsburgh, PA, 1998.

Table 2. UB3LYP/6-31+G(d,p)//UHF/6-31G(d) Energetics of Intramolecular Additions of Acyl-Substituted Radicals to Alkenes^a

reactant	6-endo pathway		5-exo pathway			endo/exo (expt)	endo/exo (calcd)
	chair TS	boat TS	chair TS	boat TS	twist-boat TS		
9	10.0	16.5	13.3	12.6	14.7	97:3 ⁷	98:2
10	12.6	19.1	15.9	14.4	16.6	—	95:5
11	8.6	15.2	15.8	14.7	16.4	—	>99:<1
12	10.9	17.2	12.7	12.1	14.1	75:25 ⁷	84:16
13	15.4	—	18.7	18.0	—	—	99:1

^a Energies are presented in kcal/mol. The reactant in all-anti conformation is taken as reference.

**Figure 1.** Transition states for the cyclization of alkyl radical **5**.

For the alkyl-substituted radical intramolecular addition reactions (**5**, **6**, **7**, and **8**), chair and boat transition states were found for the 6-endo and the 5-exo pathways. The chair transition state is usually ~2 kcal/mol lower in energy than its boat counterpart (Table 1). The average length of the forming single bond is 2.25 Å for the 6-endo pathway and 2.19 Å for the 5-exo pathway (Figure 1). The activation energy of 6.4 kcal/mol calculated for the cyclization of **5** is in good agreement with the experimental value of 6.9 kcal/mol.¹⁷ Generally speaking, the 5-exo pathway is preferred. The results for **6** and **8** indicate that alkyl substitution at C1 or C6 will not change this preference. However, as indicated by the reaction of **7**, alkyl substitution on C5 changes the preferred site of cyclization and favors the 6-endo product.

For the acyl-substituted radical intramolecular addition reactions (**9**, **10**, **11**, and **12**), chair and boat transition states were again found for the 6-endo pathway; the chair is preferred (Table 2). The average length of the forming bond is 2.19 Å (Figure 2). For the 5-exo pathway, a twist-boat transition state was also found; of the three possible transition states, the boat conformation is lowest in energy (Table 2). The average length of the forming bond is 2.15 Å for the 5-exo pathway (Figure 2). According to the computational results, the 6-endo pathway is

Table 3. UB3LYP/6-31+G(d,p)//UHF/6-31G(d) Energetics (kcal/mol) for the Haney and Curran Reactions^a

reaction	reactant	TS1	intermediate	TS2	product	
6-endo	15b	0.0	12.2	-2.3	8.0	-8.9
	16b	0.0	11.0	-4.2	9.9	-4.8
	17b	0.0	19.0	7.1	9.1	-10.6
5-exo	18b	0.0	19.2	5.5	16.7	-0.8
	19b	0.0	17.7	5.9	15.8	-0.9
	20b	0.0	21.1	7.2	13.1	-12.7

^a The two favored kinetic pathways are in boldface (corresponding to experimental results) while thermodynamically favored products are underlined.

Table 4. UB3LYP/6-31+G(d,p)//UHF/6-31G(d) Energetics (kcal/mol) for the Jung and Rayle Reactions^a

reaction	reactant	TS1	intermediate	TS2	product	
6-endo	15a	0.0	13.2	-4.6	4.7	-14.7
	16a	0.0	12.1	-5.2	7.0	-12.0
	17a	0.0	16.1	0.0	7.7	-16.0
5-exo	18a	0.0	14.5	-1.4	8.0	-10.2
	19a	0.0	14.5	-2.2	7.9	-9.5
	20a	0.0	16.6	0.7	4.3	-17.9

^a The two favored kinetic pathways are in boldface while thermodynamically favored products (corresponding to experimental results) are underlined.

always favored, whether there is alkyl substitution at C1, C5, or C6 (Table 2). For all of these simple system, there is excellent agreement between the computational results and available experimental data.

For the acyl-substituted radicals, the bond between the radical (C1) and the carbonyl group (C2) is a partial double bond of an oxyallyl radical (Figure 3). When a C1 substituent is present, it can adopt an (*E*)- or a (*Z*)-geometry. To make a comparison between *E* and *Z* conformers, the reaction of **13** was studied.

On the basis of the computational results (Table 2), the *E*-configured transition state (from **13**) is much higher in energy than its *Z*-configured counterpart (from **10**). Even in the case of *E*-configuration, the 6-endo pathway is still favored.

Experimentally determined regioselectivities are available for six model reactions, i.e., the cyclizations of **5**, **6**, **7**, **8**, **9**, and **12**, although the reaction corresponding to **8** has a 3-butenyl substituent rather than a methyl substituent on the olefin.^{3,7} Generally speaking, these calculations reproduce the experimental results very closely (Tables 1 and 2).

(2) Study of the Jung and Rayle and the Haney and Curran Intramolecular Radical Additions. We have studied in detail the possible pathways for the reactions examined by Jung and Rayle and by Haney and Curran (Scheme 6). Since such a radical addition reaction may take a 6-endo or 5-exo pathway and C1 and C5 are potential chiral centers, there are six possible pathways in both cases.

The reactions leading to **15**–**20** were studied by ab initio and density functional calculations. The reactants, transition states of the first step (TS1), intermediates, transition states of the second step (TS2), and final radical products of these reactions were determined at the UB3LYP/6-31+G(d,p)//UHF/6-31G(d) level.

The energetics of the various reactions are listed in Tables 3 and 4. As with the model reactions, there could be chair, boat and twist-boat conformations for each reaction, but for the sake of convenience, only the conformation found to be lowest in energy in the model studies was computed.

- (14) Beckwith, A. L. J.; Blair, I. A.; Phillipou, G. *Tetrahedron Lett.* **1974**, *15*, 2251–2254.
 (15) Beckwith, A. L. J.; Lawrence, T. *J. Chem. Soc., Perkin Trans. 2* **1979**, 1535–1539.
 (16) Based upon the reaction for an olefin with a 3-butenyl substituent in place of the methyl substituent in **8**, data from ref 14.
 (17) Chatgililoglu, C.; Ingold, K. U.; Scaiano, J. C. *J. Am. Chem. Soc.* **1981**, *103*, 7739–7742.

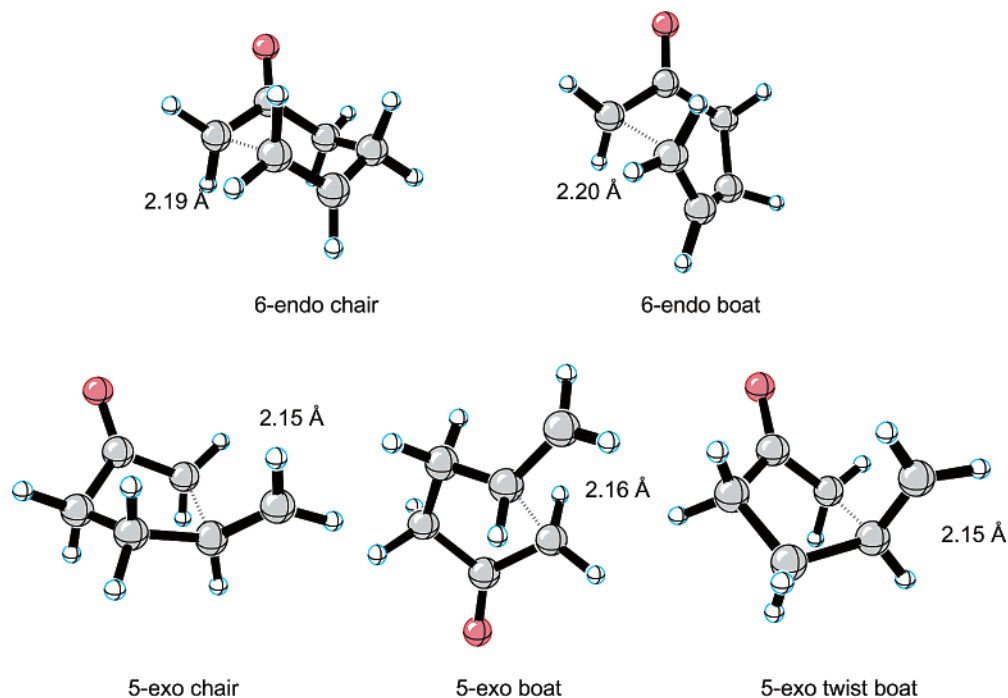


Figure 2. Transition states for the cyclization of endo-carbonyl-substituted radical **9**.

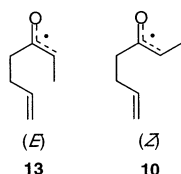


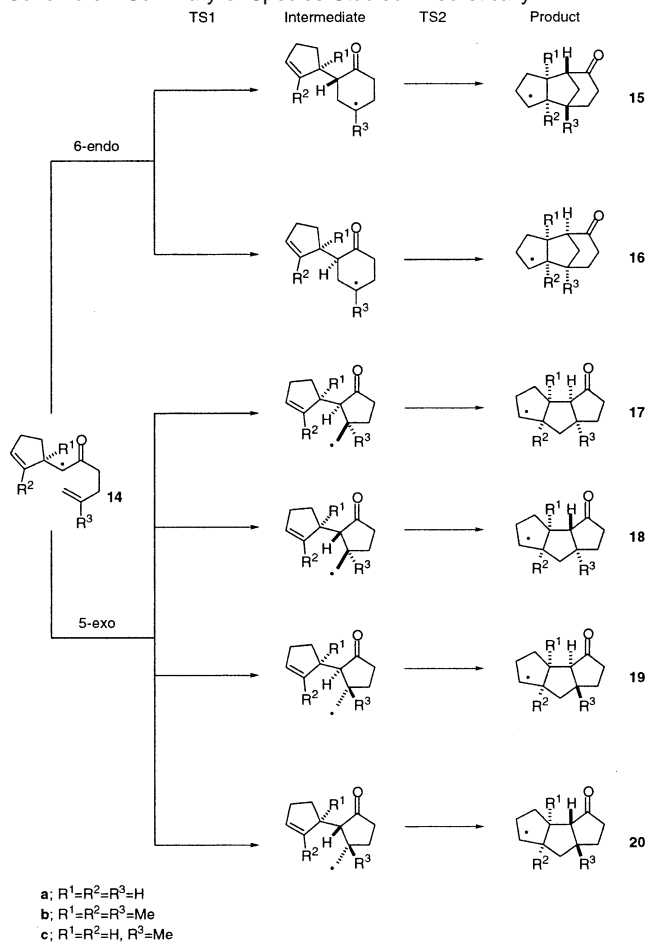
Figure 3. Substrates for the radical cyclization with an (*E*) or (*Z*) configuration about the partial double bond between the carbonyl and the radical center.

The data in Table 3 allow the observations of Haney and Curran to be interpreted. The reaction is under kinetic control with the preference being determined in the first cyclization—each product from this cyclization can only go on to form one product which occurs with a lower barrier than that for the first cyclization. The activation barriers for the four 5-exo pathways are 5–10 kcal/mol higher than the ones for the 6-endo pathways. For the 6-endo pathways, the observed preference for product **16b** (1.5 times that for **15b**) corresponding to a difference in activation energies of 0.2 kcal/mol can also be understood. There is a 1.2 kcal/mol lower barrier calculated for **16b** than for **15b** which, although a larger difference than is seen experimentally, comprises excellent agreement considering the simplifications introduced during the calculations. These results agree with Curran's interpretation and the literature on simple acyl radical cyclizations.

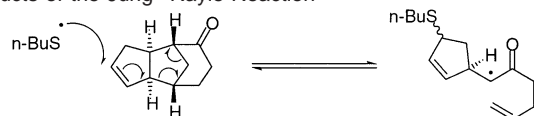
Reactions performed under Haney and Curran's conditions are likely to be under kinetic control as the product radical must abstract a hydrogen atom from a molecule of tin hydride to maintain the radical chain. The reduced product thus generated cannot participate further in the reaction. The barriers to reversion from the product are significant, and as a result the abstraction will be much faster than reversion. The production of significant amounts of side products derived from hydrogen abstraction by some of the intermediate radical species attests to the importance of this process.

The results of the reaction studied by Jung and Rayle are not

Scheme 6. Summary of Species Studied Theoretically



so straightforward to interpret. As indicated by the data in Table 4, the difference in the activation barrier for the 6-endo and the 5-exo reaction pathways (the first step) is smaller (2–3 kcal/mol) than for Haney and Curran's reaction. This is still sufficient

Scheme 7. Proposed Mechanism for the Equilibration of the Products of the Jung–Rayle Reaction**Table 5.** Calculated Energies of the Product Alkenes of the Jung–Rayle Reaction (Relative to Lowest in Each Series)^a

reaction	B3LYP/6-31+G**// HF/6-31G*	B3LYP/6-31G**// B3LYP/6-31G*
6-endo	15a'	2.9
	16a'	3.8
	17a'	3.3
5-exo	18a'	7.6
	19a'	8.2
	20a'	0.0
		0.0

^a Thermodynamically preferred products are underlined.

to conclude that the 6-endo path would be observed almost exclusively if the reaction were under kinetic control with no steps being reversible. However, the reaction is performed under extended irradiation over the course of a number of weeks. Therefore, it is not unreasonable that the product is attacked by a thiyl radical and that the intermediate radical could revert to the acyl-substituted radical intermediate (Scheme 7).

If this were the case, the product mixture would turn over slowly from the 6-endo product, through the reactant **14a**, to form an equilibrium mixture of the product alkenes, and the product ratio would be determined by the energy of the products. The alkenes corresponding to the removal of H[•] from **15a** through **20a** (denoted **15a'**–**20a'**) were therefore studied both with the UB3LYP//UHF method used previously and with UB3LYP/6-31G**//UB3LYP/6-31G*. The energies of these alkenes are reported in Table 5.

Both levels of theory predict that **20a'** is the lowest-energy product. This is in accord with the experimentally observed major product. Both methods predict that the 6-endo product, **15a'**, and the 5-exo product, **17a'**, are close in energy. The prediction based on B3LYP//B3LYP is in accord with the experimentally observed outcome that **20a'** is obtained in 47% yield and **17a'** is obtained in 26%. It may be that the remaining 27% contains some of the next favored product **15a'**.

(3) Prediction of the Possible Outcomes of an Experimentally Untried Reaction. Finally, the as-yet unreported cyclization of the methyl-substituted olefin **14c** was studied. It is known, and was confirmed by our model calculations on compound **11**, that such substitution favors the 6-endo cyclization. All of the important transition states and intermediates were optimized as before, but alongside these calculations, the same structures were optimized with the alternative density functional method. The results of all of these calculations are shown in Tables 6 and 7. The energetics obtained with both methods are in good agreement with one another, suggesting that both methods may be suitable for tackling these types of reactions. This also gives us confidence that the results obtained during the earlier studies when only one method was utilized are realistic.

As expected, the barrier for 6-endo cyclization is lowered with the methyl substituent present, since the product of this step is now a tertiary radical, whereas the barrier for 5-exo cyclization is raised due to the increased crowding along the

Table 6. Calculated UB3LYP/6-31+G**//UHF/6-31G* Energetics (kcal/mol) for the Reactions of **14c**^a

reaction	reactant	TS1	intermediate	TS2	product
6-endo	15c	0.0	11.8	-6.0	3.2
	16c	0.0	10.9	-6.7	5.3
	17c	0.0	19.2	3.4	9.8
5-exo	18c	0.0	17.2	2.5	11.9
	19c	0.0	17.0	2.4	14.3
	20c	0.0	19.4	3.8	7.4

^a The two favored kinetic pathways are in boldface while thermodynamically favored products are underlined.

Table 7. Calculated UB3LYP/6-31G**//UB3LYP/6-31G* Energetics (kcal/mol) for **14c**^a

reaction	reactant	TS1	intermediate	TS2	product
6-endo	15c	0.0	11.5	-8.7	1.3
	16c	0.0	10.7	-9.3	3.1
	17c	0.0	19.1	1.7	9.1
5-exo	18c	0.0	16.9	0.8	11.0
	19c	0.0	16.7	0.7	13.2
	20c	0.0	19.4	2.0	6.5

^a The two favored kinetic pathways are in boldface (corresponding to experimental results) while thermodynamically favored products are underlined.

Table 8. Energies of the Product Olefins for the Cyclization of Methyl-Substituted Olefin **14c**^a

reaction	UB3LYP/6-31+G**// UHF/6-31G*	UB3LYP/6-31G**// UB3LYP/6-31G*
6-endo	15c'	0.0
	16c'	2.5
	17c'	2.1
5-exo	18c'	9.7
	19c'	13.1
	20c'	0.4

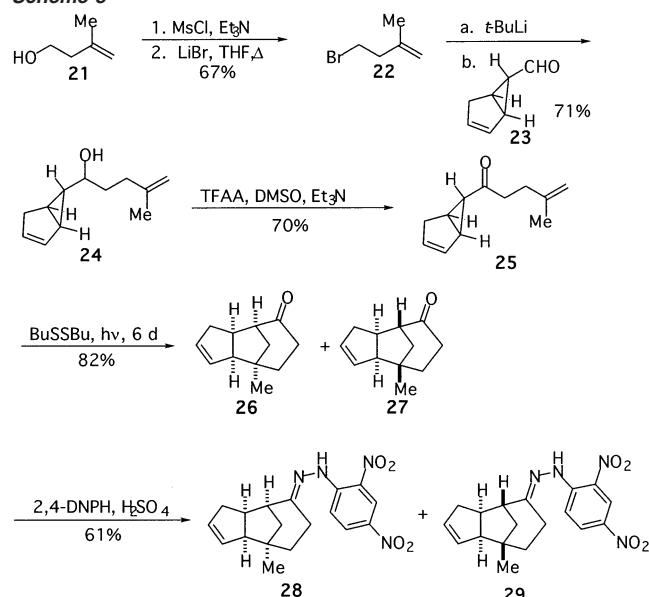
^a Thermodynamically preferred products are underlined.

forming bond in the transition state. The 6-endo products should be formed more rapidly than for the monosubstituted olefin **14a**, but they should also reverse more readily to regenerate reactant **14c**. The difference in barrier heights between 6-endo and 5-exo is in the range 5–9 kcal/mol, similar to the difference calculated for the Haney and Curran reaction. Thus, were the reaction under kinetic control, the two 6-endo products **15c** and **16c** should be the major products. By contrast, if the reaction is able to equilibrate, this will take place more slowly than for the reaction of **4**, modeled by **14a**, due to the higher barriers for the 5-exo paths. To predict the expected product mixture if this process takes place, the product olefins were also studied, and their energies are reported in Table 8.

Interestingly, in this case, both methods predict the same ordering of products and lead us to expect that at equilibrium, the major product should be the 6-endo product **15c'**. The 5-exo product **20c'** should be the next most significant and form to almost the same extent as **15c'**. The other low-energy 5-exo product, **17c'**, and the 6-endo product, **16c'**, might also be observed.

(4) Synthesis and Experimental Study of the Cyclization of Methyl-Substituted Olefin **14c.** The synthesis of the compounds corresponding to the radical **14c** begins with the conversion of 3-methyl-3-buten-1-ol to the corresponding bromide **22**, as shown in Scheme 8. The bromide was treated with *tert*-butyllithium to generate the anion which was immediately coupled to the known exo-aldehyde **23**.⁹ The resulting

Scheme 8



alcohol (**24**) was oxidized to the ketone **25**, which was subsequently photolyzed in the presence of butyl disulfide. The progress of the reaction was monitored by GC, and after 6 days the reaction was complete. Characterization and assignment of the isolated compounds (**26**, **27**) proved to be more difficult than originally anticipated, and after a number of IR and NMR methods were ruled out, the dinitrophenyl hydrazones (**28**, **29**) were synthesized. Fortunately, the hydrazones were crystalline, and the structures could be identified unambiguously from the X-ray analysis, Figure 4.

The X-ray structure clearly shows the product is a mixture of 6-endo products. The structure in black, the *cis-syn-cis* product **28** corresponding to **16c** is the major isomer constituting 82% of the crystal, while the white structure, the *cis-anti-cis* product **29** corresponding to **15c** is the minor component found in 18%. GC and ¹H NMR data show that the ratio of major to minor products is 1.7:1, corresponding to a $\Delta\Delta E^\ddagger$ of ~ 0.3 kcal/mol. This closely parallels the Haney–Curran work, wherein a 1.5 to 1 ratio of major to minor 6-endo products corresponding to **16b** and **15b** was observed. Our calculations had shown that kinetic control should yield a mixture of **16c** and **15c**, and thermodynamic control, **15c** and **20c**. The experimental observations are consistent with kinetic control even though the same conditions had previously provided thermodynamic control for the cyclization of **4**.

To rationalize the switch from thermodynamic to kinetic control, the computed energetics for **14c** were contrasted with those computed for **14a**, which modeled the cyclization of **4**. The difference in barrier heights between 6-endo and 5-exo cyclizations was 1–5 kcal/mol for **14a** but 5–9 kcal/mol for **14c**. This significant change in relative barriers for 6-endo and 5-exo makes the 5-exo products kinetically less easily accessible. Equilibration of **14c** would be much slower than for **14a**. Indeed, degradation may become competitive with the equilibration—this is suggested and supported by the experimental observation that the baseline of the GC chromatogram becomes crowded with small peaks as the photolysis progresses.

A further aspect of note is the change in reaction times on going from **4**, which took 3 weeks to **25**, which took just 6

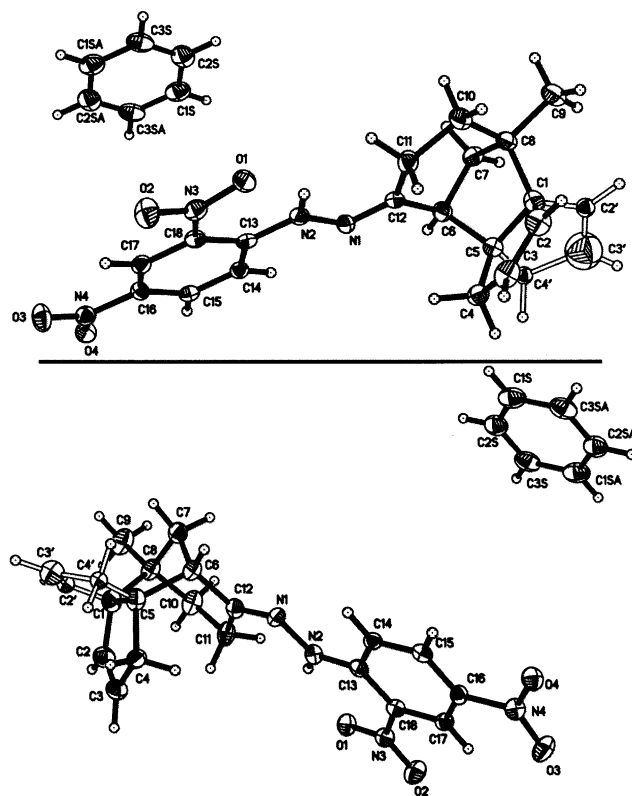


Figure 4. X-ray crystal structure of the 2,4-dinitrophenylhydrazone derivatives of the product of the reaction in which **25** is subjected to the Jung and Rayle conditions for radical cyclization. The crystal is composed of a mixture of two isomers, **28** and **29**, represented by white and black structures in the region where the two structures diverge.

days. This is consistent with the calculated barrier heights which are lower for 6-endo cyclization for **14c** (10.9 and 11.8 kcal/mol) than for **14a** (12.1 and 13.2 kcal/mol). The barriers for subsequent equilibration to 5-exo products show the opposite trend and are lower for **14a** which subsequently undergoes equilibration.

The barriers calculated for **14c** are similar to those for **14b**, which had been used to model the Haney–Curran reaction of **1**. The difference between barriers for 6-endo and 5-exo cyclizations is 5–10 kcal/mol for **14b**. The reaction of **1** was performed under conditions that ensured the observation of kinetic products. The computed energetics suggest that, if a reaction is performed on the analogous substrate under the Jung–Rayle conditions, the same kinetically determined products should be observed.

Conclusions

Ab initio and density functional calculations have been used to rationalize and to predict the outcome of radical reactions. The calculations mirror the outcome of simple model reactions and are useful in interpreting the studies of more complex systems.

In a radical cyclization reported by Haney and Curran, calculations are consistent with a selectivity determined by kinetic control; the difference in activation energies favors 6-endo cyclization over the alternative 5-exo cyclization by 5 to 10 kcal/mol.

The radical cyclization reported by Jung and Rayle is explained as being reversible under the reaction conditions with

the products being determined by thermodynamic stability. The difference in activation energies still favors 6-endo cyclization, but only by 1–5 kcal/mol.

A prediction was made for the outcome of a related reaction which was performed under the Jung and Rayle conditions but which experimental testing showed yielded products determined by kinetic control. This reaction demonstrates the subtle balance involved in the energetics determining the outcome of these reactions. The difference in activation barriers between 6-endo and 5-exo cyclization was 5–9 kcal/mol in this case.

Experimental Section.

General. All ^1H NMR spectra were obtained on a Bruker ARX-400 spectrometer operating at 400.132 MHz, a Bruker ARX-500 spectrometer operating at 500.132 MHz, or a Bruker Avance-500 spectrometer operating at 500.330 MHz as indicated. All ^{13}C NMR spectra were recorded on a Bruker ARX-400 spectrometer operating at 100.625 MHz, a Bruker ARX-500 spectrometer operating at 125.773 MHz, or a Bruker Avance-500 spectrometer operating at 125.808 MHz. All ^1H and ^{13}C NMR data are reported in parts per million (δ) downfield from tetramethylsilane. Coupling constants are reported in hertz (Hz), with the following abbreviations used: s = singlet, d = doublet, t = triplet, q = quartet, m = multiplet. When appropriate, the multiplicities are preceded with b, indicating that the signal is broad.

FTIR spectrometry was performed on a Nicolet-501 FTIR spectrometer using liquid films (neat) on NaCl plates, and only the most significant absorption bands are reported in cm^{-1} . High-resolution mass spectra (HRMS) were recorded on a VG Analytical Autospec double-focusing instrument using the electron impact (EI) technique. Gas chromatographic analyses were performed using a Hewlett-Packard 5790A series chromatograph with an SE-30 cross-linked methyl silicone gum column (12 m \times 0.2 m \times 0.33 mm film thickness). Photolysis was done using a Hanovia model 73A36 550 W medium-pressure mercury lamp at room temperature.

Thin-layer chromatography (TLC) was carried out using Baker Si250F₂₅₄ silica gel plates and visualization was facilitated by the use of ultraviolet light, anisaldehyde stain, phosphomolybdic acid stain, permanganate stain, vanillin stain, or iodine chamber methods. Flash chromatography was performed using E. Merck silica gel 60 (230–400 mesh) with compressed air as the source. All solvent mixtures used are indicated as percentages.

The following solvents were dried and distilled from the indicated drying agent under an argon atmosphere: tetrahydrofuran (THF) and diethyl ether from sodium benzophenone ketyl radical; dichloromethane, benzene, toluene, hexane, pyridine, and triethylamine from calcium hydride; diisopropylamine from sodium hydroxide; methanol from magnesium methoxide. All other solvents and reagents were purified and dried before use as necessary by standard techniques.

4-Bromo-2-methyl-1-butene, 22. To an oven-dried round-bottomed flask charged with a stir bar and dichloromethane (200 mL) was added 3-methyl-3-buten-1-ol (10.0 mL, 99.0 mmol), and the solution was cooled to 0 °C, and triethylamine (21.0 mL, 148.6 mmol) was added. To the stirring solution was added dropwise a solution of methanesulfonyl chloride (MsCl, 11.6 mL, 148.6 mmol) in dichloromethane (50 mL) via addition funnel. The reaction was allowed to stir for 1 h while warming to room temperature, and was then quenched by the addition of saturated ammonium chloride (200 mL). The organic phase was washed with saturated ammonium chloride (3 \times 100 mL) and brine (100 mL) before being dried over MgSO_4 . After filtration, the resulting solution was reduced in vacuo in the dark to produce a clear oil. This oil was dissolved in THF (125 mL), and dry lithium bromide (17.0 g, 198.1 mmol) was added. The suspension was heated at reflux for 12 h and cooled to 25 °C, and water (100 mL) was added. The organic phase was washed with brine (100 mL) and then dried over MgSO_4 . After filtration, the resulting solution was reduced in vacuo in the dark to

give 9.86 g (67%) of the bromide **22** as a light-sensitive, clear oil. ^1H NMR (CDCl_3 , 400 MHz) δ 4.85 (1H, d, $J = 0.7$ Hz), 4.76 (1H, d, $J = 0.7$ Hz), 3.44 (2H, t, $J = 7.4$ Hz), 2.57 (2H, t, $J = 7.4$ Hz), 1.74 (3H, s). ^{13}C NMR (CDCl_3 , 100 MHz) δ 142.4, 112.7, 40.9, 30.8, 21.9.

($\alpha\text{RS},1\text{R},5\text{R},6\text{S}$)- α -(3-Methyl-3-butenyl)-bicyclo[3.1.0]hex-2-ene-6-methanol, 24. To an oven-dried round-bottomed flask charged with a stir bar and diethyl ether (10 mL) was added *tert*-butyllithium (2.0 M in pentanes, 2.22 mL, 5.6 mmol), and the solution was cooled to –90 °C. To this solution was added dropwise a solution of the bromide **22** (0.51 g, 2.8 mmol) in diethyl ether (5 mL) via syringe pump, and the reaction was allowed to stir for 20 min. To this solution was then added a solution of the aldehyde **23** (0.20 g, 1.85 mmol) in diethyl ether (5 mL), and the reaction was allowed to stir until TLC indicated completion (ca. 0.5 h). The reaction was quenched by pouring the cold solution into water (30 mL). The organic layer was washed with saturated sodium bicarbonate (30 mL) and brine (30 mL) before being dried over MgSO_4 . After filtration, the resulting solution was reduced in vacuo, and the oil was purified by flash chromatography (silica gel, 15% diethyl ether in pentane) to give 0.35 g (71%) of the alcohol **24** as a 1:1 mixture of diastereomers. ^1H NMR (CDCl_3 , 500 MHz) δ 5.89 (1H, m), 5.42 (1H, m), 4.71 (2H, bs), 2.97 (1H, m), 2.58 (1H, m), 2.37 (1H, m), 2.13 (2H, m), 1.89 (1H, m), 1.74 (5H, m), 1.65 (1H, m), 1.53 (1H, m), 0.38 (1H, m). ^{13}C NMR (CDCl_3 , 125 MHz) δ 145.9, 145.8, 133.5, 133.1, 129.0, 128.6, 110.0, 109.9, 74.5, 74.1, 36.6, 36.0, 35.8, 35.6, 35.0, 34.7, 34.0, 33.9, 29.3, 28.9, 22.6 (2C's), 20.7, 20.3.

1-[(1R,5R,6S)-Bicyclo[3.1.0]hex-2-en-6-yl]-4-methyl-pent-4-en-1-one, 25. To an oven-dried round-bottomed flask charged with a stir bar and dichloromethane (20 mL) was added trifluoroacetic anhydride (0.48 mL, 3.4 mmol), and the reaction was cooled to –78 °C. To the stirring solution was added dimethyl sulfoxide (DMSO, 0.48 mL, 6.7 mmol) with venting, and the reaction was allowed to stir for 0.5 h. To the stirring solution was then added the alcohol **24** (0.20 g, 1.1 mmol) in dichloromethane (3 mL), and the reaction was allowed to stir for 1 h. Triethylamine (1.41 mL, 10.1 mmol) was then added, and the reaction was allowed to warm to 0 °C before the addition of saturated ammonium chloride (30 mL). The organic layer was washed with saturated ammonium chloride (3 \times 30 mL) and brine (30 mL) before being dried over MgSO_4 . After filtration, the resulting solution was then reduced in vacuo, and the oil was purified by flash chromatography (silica gel, 20% diethyl ether in pentane) to give 0.136 g (70%) of the ketone **25** as a clear oil. ^1H NMR (CDCl_3 , 500 MHz) δ 5.98 (1H, m), 5.62 (1H, m), 4.77 (1H, s), 4.71 (1H, s), 2.82 (1H, m), 2.72 (2H, t, $J = 7.6$ Hz), 2.49 (2H, m), 2.33 (2H, t, $J = 7.6$ Hz), 2.29 (1H, m), 1.77 (3H, s), 1.34 (1H, m). ^{13}C NMR (CDCl_3 , 125 MHz) δ 209.0, 144.5, 132.3, 130.6, 110.0, 41.7, 38.6, 37.2, 36.4, 31.6, 28.7, 22.5. IR (neat) 2910, 1690, 1390, 1370, 1180, 1100 cm^{-1} .

(3aR,4S,8R,8aS)-8-Methyl-3a,4,6,7,8,8a-hexahydro-3H-4,8-methanoazulen-5-one, 26, and (3aR,4R,8S,8aS)-8-Methyl-3a,4,6,7,8,8a-hexahydro-3H-4,8-methanoazulen-5-one, 27. To an oven-dried round-bottomed flask charged with a stir bar and benzene (5 mL) was added the ketone **25** (91 mg, 0.52 mmol) and *n*-butyl disulfide (69 μL , 3.6 mmol). The solution was degassed using five freeze–pump–thaw cycles and was then photolyzed until analysis by GC indicated all the starting ketone had been consumed (ca. 6 d). The reaction mixture was then reduced in volume to approximately 1 mL and directly loaded onto a silica gel column. Flash chromatography (10% diethyl ether in pentane) gave 75.2 mg (82%) of the ketones **26** and **27** as an inseparable mixture. The ratio of the major product **26** to the minor product **27** was 1.7:1 (**26**, 52%; **27**, 30%). ^1H NMR (CDCl_3 , 500 MHz) δ **26**: 5.77 (1H, m), 5.62 (1H, m), 2.97 (1H, bs), 2.75 (2H, m), 2.49 (1H, m), 2.38 (1H, d, $J = 4.4$ Hz), 2.19 (1H, m), 2.03 (1H, m), 1.74 (3H, m), 1.64 (1H, m), 1.04 (3H, s). **27**: 5.83 (1H, m), 5.75 (1H, m), 3.05 (2H, m), 2.76 (1H, m), 2.49 (1H, m), 2.26 (1H, bd, $J = 6.9$ Hz), 2.17 (1H, m), 2.05 (1H, m), 1.87 (1H, m), 1.64 (3H, m), 1.20 (3H, s). Mixture of **26** and **27**: ^{13}C NMR (CDCl_3 , 125 MHz) δ 214.3 (2C's), 132.4, 131.9,

131.0, 130.3, 60.1, 58.9, 58.3, 55.7, 45.7, 43.8, 43.7, 42.5, 40.8, 39.9, 39.1, 36.0, 35.2, 34.1, 33.9, 27.0, 22.4, 15.3.

IR (neat) 3050, 2930, 2861, 1713, 1460 cm^{-1} . HRMS (EI) 175.112037 calcd for $\text{C}_{12}\text{H}_{16}\text{O}$ 175.112290.

N-(2,4-Dinitrophenyl)-*N'*-[(3*aR*,4*S*,8*R*,8*aS*)-8-Methyl-3*a*,4,6,7,8,8*a*-hexahydro-3*H*-4,8-methanoazulen-5-ylidene]hydrazine, **28**, and *N*-(2,4-Dinitrophenyl)-*N'*-[(3*aR*,4*R*,8*S*,8*aS*)-8-Methyl-3*a*,4,6,7,8,8*a*-hexahydro-3*H*-4,8-methanoazulen-5-ylidene]hydrazine, **29**. To a solution of ethanol (25 mL), water (7 mL), and sulfuric acid (concentrated, 7 mL) was added 2,4-dinitrophenyl hydrazine (1.0 g, 5.0 mmol), and the mixture was stirred. This solution (6.6 mL) was then added to a solution of the ketones **26** and **27** (0.10 g, 0.57 mmol) in ethanol (2 mL) which immediately formed an orange precipitate. The reaction was allowed to stir for 0.5 h before filtering the mixture to give an orange solid. The solid was washed with saturated sodium bicarbonate (3×50 mL) and water (3×50 mL) to give a crude orange solid. The solid was dissolved in a minimum amount of diethyl ether and purified by flash column chromatography (silica gel, 33% diethyl ether in pentane) to give 124 mg (61%) of the hydrazones **28** and **29** as an orange powder. X-ray quality crystals were grown by the slow evaporation of a 1:1 mixture of benzene and 1,2-dichloroethane. ^1H NMR (CDCl_3 , 500 MHz) δ Major, *cis*-*syn*-*cis*, **28**: 11.0 (1H, s), 9.12 (1H, d, $J = 2.5$ Hz), 8.28 (1H, dd, $J = 9.5, 2.5$ Hz), 7.97 (1H, d, $J =$

9.5 Hz), 5.77 (1H, m), 5.68 (1H, m), 3.14–1.24 (11H, m), 1.20 (3H, s). Minor, *cis*-*anti*-*cis*, **29**: 11.1 (1H, s), 9.12 (1H, d, $J = 2.5$ Hz), 8.28 (1H, dd, $J = 9.5, 2.5$ Hz), 7.94 (1H, d, $J = 9.5$ Hz), 5.77 (1H, m), 5.62 (1H, m), 3.14–1.24 (11H, m), 1.04 (3H, s). Mixture of **28** and **29**: ^{13}C NMR (CDCl_3 , 125 MHz) δ 138.2, 132.3, 131.7, 129.8, 128.2, 123.5, 116.2, 116.1, 59.6, 57.6, 52.4, 48.6, 45.9, 45.4, 45.0, 42.6, 42.2, 40.9, 39.8, 38.2, 33.5, 33.0, 27.3, 22.1, 21.6, (imine carbon not observed). IR (neat) 3326, 3104, 3054, 2930, 2868, 1618, 1592, 1519, 1506, 1426, 1335, 1265, 739 cm^{-1} . HRMS (EI) 356.148310 calcd for $\text{C}_{18}\text{H}_{20}\text{N}_4\text{O}_4$ 356.148455.

Acknowledgment. We thank the National Institute of General Medical Sciences, National Institutes of Health for financial support, and AstraZeneca and the UK Fulbright Commission for a fellowship (to A.G.L.). This work was partially supported by National Computational Science Alliance.

Supporting Information Available: ^1H and ^{13}C NMR spectra for compounds **22** and **24–27** (PDF). An X-ray crystallographic file in CIF format. This material is available free of charge via the Internet at <http://pubs.acs.org>.

JA029342Q